AIP | Applied Physics Letters

Polyamorphism in cerium based bulk metallic glasses: Electronic and structural properties under pressure and temperature by x-ray absorption techniques

L. Belhadi, F. Decremps, S. Pascarelli, L. Cormier, Y. Le Godec et al.

Citation: Appl. Phys. Lett. **103**, 111905 (2013); doi: 10.1063/1.4820434
View online: http://dx.doi.org/10.1063/1.4820434
View Table of Contents: http://apl.aip.org/resource/1/APPLAB/v103/i11
Published by the AIP Publishing LLC.

Polyamorphism in cerium based bulk metallic glasses: Electronic and structural properties under pressure and temperature by x-ray absorption techniques

L. Belhadi,[1] F. Decremps,[1] S. Pascarelli,[2] L. Cormier,[1] Y. Le Godec,[1] S. Gorsse,[3] F. Baudelet,[4] C. Marini,[2] and G. Garbarino[2]
[1]*IMPMC, Université Pierre et Marie Curie, 75252 Paris, France*
[2]*ESRF, F-38043 Grenoble, France*
[3]*CNRS, ICMCB, Université de Bordeaux, F-33600 Pessac, France*
[4]*Synchrotron SOLEIL, F-91192 Gif Sur Yvette, France*

(Received 3 July 2013; accepted 29 July 2013; published online 10 September 2013)

High pressure and high temperature x-ray absorption near edge spectroscopy experiments have been carried out on $Ce_{60}Al_{20}Cu_{20}$ bulk metallic glass showing an electronic delocalization of the 4f-electron of cerium under pressure. In parallel, high pressure extended x-ray absorption fine structure spectroscopy reveals large structural modifications of the cerium local environment. This study provides experimental evidence that an electronic driven structural transformation occurs in cerium based bulk metallic glasses (Ce-BMGs). The effect of temperature on the hysteresis of this amorphous-amorphous phase transition is also discussed, suggesting the existence of a critical point in the phase diagram of Ce-BMGs. This work will encourage further investigations on Ce-based metallic glasses phase diagrams in order to support, or refute, the actual theoretical understanding of polyamorphism. © *2013 AIP Publishing LLC*.
[http://dx.doi.org/10.1063/1.4820434]

Bulk Metallic Glasses (BMGs) are amorphous materials which combine the electric conductivity of metals with glassy structural disorder, thus promising to be industrial products with outstanding performance.[1–3] Recently, rare earth based metallic glasses including cerium based BMGs (Ce-BMGs) have been found to display thermo-plastic behavior with very low glass transition temperature ($T_g < 373$ K) and low Young's modulus in comparison to classical amorphous matter.[4–6] At room temperature, these alloys are strong (elastic strain of 2% (Ref. 4)) and brittle. In their supercooled-liquid state, these materials can, however, be repeatedly shaped into very fine structures down to the nanometer-scale, of great interest for micro-electromechanical systems or nano-technology applications such as high density data storage.[7]

In this context, the structural,[8–10] electronic,[11,12] elastic,[13–15] and thermal[16] properties of Ce-BMGs have been extensively studied. Under pressure, an amorphous-amorphous phase transition occurs from a low density amorphous phase (LDA) to a high density amorphous phase (HDA). Indeed, x-ray diffraction (XRD) measurements on Ce-BMGs[8,12,14] have shown an important change of density under pressure (almost 15%). This pressure-induced-volume change is reversible and exhibits hysteresis under decompression. Sheng *et al.* have proposed a structural model for the LDA and HDA phases based on *ab initio* molecular dynamics simulations[8] in which a splitting of the Ce-Ce nearest-neighbors distance is observed at the transition. The local structure at high pressure exhibits a double shell feature, with an inner shell corresponding to a significant shorter bond compared to the low pressure structure. In these calculations, the LDA and HDA phases have been characterized, respectively, by a localized and itinerant 4f electron.

X-ray absorption near-edge spectroscopy experiments on amorphous $Ce_{75}Al_{25}$ (Ref. 12) have indeed confirmed a 4f-electron delocalization related to an important densification under pressure. 4f electronic delocalization is also observed in pure cerium and is responsible for the $\gamma \leftrightarrows \alpha$ transition.[17,18] Since polyamorphism in lanthanide BMGs is related to the behavior of 4f electrons in solvent metals,[19] the link between polyamorphism in Ce-BMGs and the $\gamma \leftrightarrows \alpha$ transition in cerium appears evident. Owing to the remarkable properties of the $\gamma \leftrightarrows \alpha$ transition (large volume collapse, existence of a critical point (CP) at the end of this transition line, or an atypical mechanism[20]), polyamorphism in Ce-BMGs is then expected to generate quite unusual important structural modifications.[21]

Insight into the nature of this polyamorphism in terms of changes in the local structure or order of the transition is a remaining issue. Indeed, the "classical" amorphous-amorphous structural phase transitions earlier reported in covalent glasses with low coordination number (CN) and directional bonding (ice,[22] silica[23]) involves a topological rearrangement of atoms driven by an increase of CN under pressure. By contrast, BMGs local structures are highly compact[24] with non-directional bonding (metal): no structural polyamorphism is thus expected in these systems within the paradigm proposed for open structure amorphous compounds. The observation of an electronic-driven polyamorphism in Ce-based BMGs may be associated with a local rearrangement and a structural transition that has not been yet experimentally observed. The numerical simulations by Sheng *et al.* represent the unique attempt to identify the structural modifications of a Ce-BMG under pressure. But the local density approximation used to simulate the experimental x-ray structure factor is well known[25] to not

reproduce the electronic correlations in cerium. The validity of the structural model proposed by Sheng *et al*. thus needs to be confirmed by an experimental method for which analysis does not require any hypothesis on 4f-electronic states.

In this work, we present combined investigation of electronic and structural properties of $Ce_{60}Al_{20}Cu_{20}$ BMG at high pressure and high temperature by x-ray absorption spectroscopy (XAS) techniques. Energy dispersive x-ray absorption near edge spectra (XANES) show a pressure-induced delocalization of the Ce 4f-electron characterized by a smoothing out of the hysteresis loop upon temperature increase. High pressure extended x-ray absorption fine structure (EXAFS) spectra highlight structural changes with respect to ambient and provide a test on the validity of the structural model proposed by Sheng *et al*.

$Ce_{60}Al_{20}Cu_{20}$ metallic glass was prepared in the form of thin ribbons (thickness $\approx 30\ \mu$m) using the single-roller melt-spinning technique. Its compositions were confirmed by electron microprobe, scanning electron microscopy images showing uniform contrast. The glassy nature of the sample was verified by x-ray diffraction (no detectable Bragg peaks) and differential scanning calorimetry (presence of exothermic peak indicative of a glass transition temperature). Moreover, a recent high pressure XRD study[26] up to 15 GPa shows that the CN of Ce, close to 12 at ambient conditions, remains constant to within 10%.

Energy dispersive XANES were measured at the ODE (Optique Dispersive EXAFS) beamline (Synchrotron Soleil) in transmission mode with a beam size of $\sim 20 \times 20\ \mu m^2$ FWHM at the Ce L_3-edge (5.7 keV). Samples were inserted into the hole of a Cu-Be gasket with silicone oil as pressure-transmitting medium in a resistibly heated diamond anvil cell (DAC). Because of the strong absorption of diamonds at this energy, drilled anvils (of 500 μm of thickness) have been used in order to reduce the path length. Pressure values were determined using the ruby fluorescence method.[27] Compression and decompression cycles up to 9 GPa have been realized at several isotherms (with an unique sample loading for each of them) until 330 K providing information on both the electronic state and the transition kinetics.

L_3-edge x-ray spectroscopy probes the empty density of states of "d" symmetry while sensitivity to the 4f electrons arises through d–f hybridization. 4f-electron hybridization on the mixed-valent ground state, $c_0 \times |4f^0\rangle + c_1 \times |4f^1\rangle + c_2 \times |4f^2\rangle$ (c_i being their weight), is suppressed by the 2p core-hole Coulomb potential. The different components of the ground state, i.e., $|4f^0\rangle$ (itinerant), $|4f^1\rangle$ (localized), and $|4f^2\rangle$ (strong hybridization with conduction electrons), split in the XAS final states according to their weight (c_i). The 4f-electron state can then be readily characterized since the energy attributed to each $|4f^i>$ final state configuration is different (due to their respective screening effects).

Figure 1 (left) shows the XANES collected on $Ce_{60}Al_{20}Cu_{20}$ metallic glass at room temperature. At ambient pressure, the spectrum exhibits a single "white line" feature, attributed to the $|4f^1\rangle$ final state configuration (localized 4f electron). At high pressure, a hump appears about 10 eV above the white line (energy corresponding to the $|4f^0\rangle$ final state), and grows with pressure at expense of the white line intensity. The transfer of spectral weight from the $|4f^1\rangle$ to

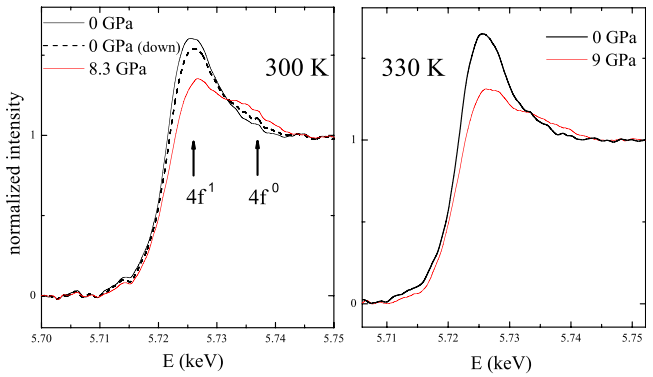

FIG. 1. Ce L_3-edge XANES of $Ce_{60}Al_{20}Cu_{20}$ metallic glass at 300 K (left) and 330 K (right). Black: ambient, red: high P, dashed: after decompression. Solid arrows mark the $|4f^0\rangle$ (itinerant) and $|4f^1\rangle$ (localized) components.

$|4f^0\rangle$ component provides here experimental evidence of the 4f-electron delocalization under pressure for amorphous $Ce_{60}Al_{20}Cu_{20}$, behavior already observed in other Ce-BMGs.[12] This electronic transition is globally reversible and is also observed for the first time at high temperature (right side of Figure 1).

To probe the local environment, EXAFS measurements at the Ce K-edge (40.4 keV) were carried out at beamline BM23 of the ESRF, with a beam size of about 70 μm (500 μm) vertically (horizontally) in transmission mode. $Ce_{60}Al_{20}Cu_{20}$ was slowly ground and homogeneously mixed with magnesium oxide (MgO) (1:3 in weights) by ball milling and then inserted into a boron nitride (hBN) cylinder. No crystallization of the sample has been observed by diffraction during this treatment. The MgO cylinder has then been loaded into a cylindrical boron-epoxy gasket and compressed between two sintered diamond anvils of a Paris-Edinburgh Press. XRD patterns of both MgO and Ce-BMGs were recorded between each EXAFS to determine *in situ* pressure and to probe the amorphous state of the sample under compression. EXAFS extraction and analysis were carried out using the FEFFIT package.[28]

Figure 2 shows the normalized absorption spectra at ambient pressure and at 8.5 GPa. The EXAFS oscillations are barely visible. This is due to the combined effect of (i) large structural disorder, typical of metallic glasses, that strongly damps the signal at large k values, and of (ii) the high energy of the Ce K-absorption edge ($E \approx 40.4$ keV), associated to a large core-hole lifetime ($\Delta E_{ch} \approx 15$ eV (Ref. 30)), that strongly damps the signal at low k values. The inset of Figure 2 shows the derivative of absorption at the edge. No significant changes in the onset of absorption are observed in this pressure range.

Figure 3 shows (a) the k^2-weighted EXAFS functions $k^2 \times \chi(k)$ and (b) the amplitude of the Fourier Transform (FT) $|\chi(R)|$ calculated for the k range of 3.0–8.5 $Å^{-1}$ at ambient pressure (black) and 8.5 GPa (red). A first qualitative analysis of this figure shows a major change in the phase of the EXAFS $k^2 \times \chi(k)$ oscillations, and a slight shift towards larger R of the main peak of the $|\chi(R)|$. Pressure evidently induces important changes in the environment of Ce that do not seem compatible with a simple compression of the ambient pressure phase.

Due to the reduced k-range available for the data analysis, and to the very small amplitude of the signal (hence leading to a reduced signal to noise ratio), it was not possible to

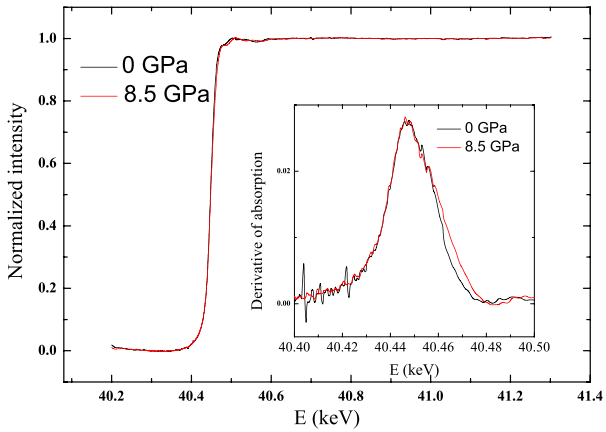

FIG. 2. Ce K-edge x-ray absorption spectrum of $Ce_{60}Al_{20}Cu_{20}$ bulk metallic glass at ambient conditions (black curve) and 8.5 GPa (red curve). Inset: Corresponding derivative of absorption at 0 GPa (black curve) and at 8.5 GPa (red curve).

identify with sufficient confidence the details of the local structure around Ce at high pressure. Our aim was therefore less ambitious and consisted in highlighting any significant difference between the ambient pressure and the high pressure data sets by carrying out a comparative analysis. Therefore, exactly the same structural models were tested on each data set. The first test was to check whether the data at high pressure could be described by a compressed form of the ambient pressure structure. If not, then the second test was to check whether the structural changes induced by pressure were compatible with a Ce-Ce split-shell model, as proposed by Sheng *et al.*[8]

The data were fitted in the R range of 1.5–3.8Å (corresponding to the first peak in the FT). The number of independent points ($N_{indpoints}$) for the fits is estimated as[31]

$$N_{indpoints} = \frac{2 \times k_{range} \times r_{range}}{\pi} + 2 = 10. \quad (1)$$

Based on the assumption that the distribution of atomic species in BMGs is random, a model with a fixed total Ce CN (12) of which 60% Ce (7.2 Ce-Ce bonds), 20% Al (2.4 Ce-Al bonds), and 20% Cu (2.4 Ce-Cu bonds) was used. Fixing the chemical composition (i.e., the Ce-X partial coordination numbers) of the first neighbours of Ce as a function of pressure is a rough approximation but consistent with previous work.[8,26]

For each neighboring atomic species X (X = Ce, Al, Cu), we used the assumption of a Gaussian distribution of atoms centered at the average bond distance R_{Ce-X}. We describe the distribution of the Ce-Ce bonds by two equally populated peaks at distances R_{Ce-Ce1} and R_{Ce-Ce2} separated by $\delta : R_{Ce-Ce2} = R_{Ce-Ce1} - \delta$ (i.e., a single Ce-Ce distance is present if $\delta = 0$, and two Ce-Ce distances if $\delta \neq 0$) and with equal mean square relative displacements (MSRDs). The parameter δ was kept fixed during the fits.

The amplitude factor S_0^2 was set to 0.9. The value of ΔE was evaluated from the ambient P data by assuming a single Ce-Ce distance ($\delta = 0$) centered at the value found in cubic Ce_3Al: $R_{Ce-Ce} = 3.54$ Å. This assumption is justified by the fact that the density of Ce-BMGs is closed to the density of their crystalline counterpart at ambient pressure,[29] so R_{Ce-Ce} is expected to be close to the Ce-Ce distance observed in a crystal with a similar chemical composition. For all fits, the ΔE parameter was fixed to this value (−15 eV).

To further reduce the number of free fitting parameters, the MSRD of Cu and Al were set equal ($\Delta\sigma^2_{Ce-Al} = \Delta\sigma^2_{Ce-Cu}$). Releasing this constraint did not significantly change the values of $\Delta\sigma^2_{Ce-Al}$ and $\Delta\sigma^2_{Ce-Cu}$. Therefore, five free parameters ($N_{freeparameters}$) were used: the three distances R_{Ce-Ce}, R_{Ce-Al}, R_{Ce-Cu} and two mean square relative displacement $\Delta\sigma^2_{Ce-Ce}$ and $\Delta\sigma^2_{Ce-Al}$. The number of degrees of freedom ν for the fits was $\nu = N_{indpoints} - N_{freeparameters} = 5$.

Within the crude structural model imposed due to the limited amount of information contained in our data—constrained by a fixed total coordination number, a fixed chemical composition and one or two equally populated and equally disordered Ce-Ce peaks—we tested a large number of possible atomic configurations, starting from a single Ce-Ce shell ($\delta = 0$) to an increasingly split Ce-Ce shell configuration ($\delta_{max} = 0.35$).

Figure 4 shows the evolution of the quality of the fits (reduced $\chi^2 : \chi^2_\nu$) as a function of the parameter δ, for both the ambient (blue) and the high pressure (red) data.

For each of these fits, while the parameter δ was kept fixed, the other five parameters adjusted their values to minimize the χ^2 function. By monitoring the values of all free parameters as a function of δ, we were able to visualize the

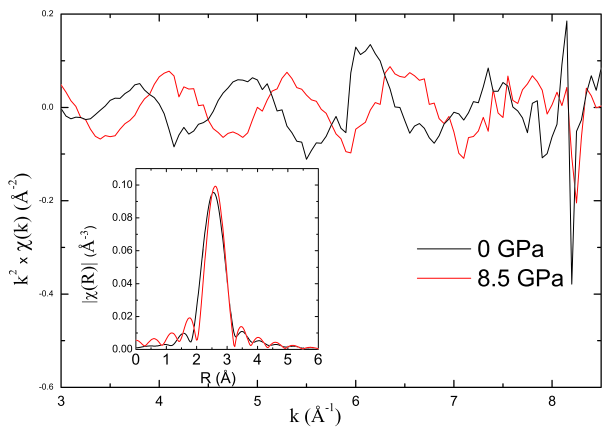

FIG. 3. $Ce_{60}Al_{20}Cu_{20}$ k^2-weighted EXAFS functions $k^2 \times \chi(k)(Å^{-2})$. Inset: the corresponding amplitude of the FT $|\chi(R)|$.

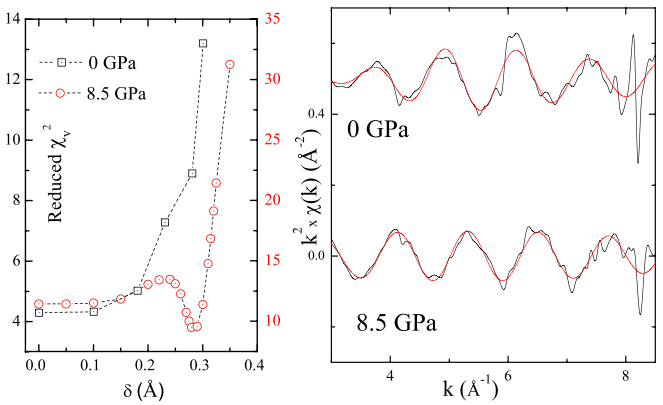

FIG. 4. Left: χ^2_ν as a function of δ parameter (splitting of the Ce-Ce distance in $Ce_{60}Al_{20}Cu_{20}$ metallic glass). Right: best fit (red) to EXAFS data $k^2 \times \chi(k)(Å^{-2})$ (black) at 0 GPa (up) and 8.5 GPa (down).

correlations between δ and the other parameters. For the high pressure (HP) fits, we find that the values of Ce-Cu distance and $\sigma^2_{Ce-Al(Ce-Cu)}$ are weakly affected by δ, while the Ce-Ce and Ce-Al distances increase (+0.05 Å and +0.15 Å, respectively). As expected, we find strong correlation between δ and σ^2_{Ce-Ce}, with the latter decreasing monotonically as δ increases.

Table I lists the best fit values of the structural parameters obtained for the ambient and the high pressure data for values of δ equal to 0 (single Ce-Ce shell) and 0.28 (split Ce-Ce shell).

From Figure 4, we note that the ambient pressure data is best reproduced with δ equal to or very close to 0. As δ increases above 0.1, the quality of the fit rapidly degrades. This is a strong indication that the ambient pressure data is best reproduced by a single Ce-Ce distance.

When we use this model ($\delta = 0$) to fit the high pressure data, the reported bond lengths (see Table I) are not compatible with a uniform compression of the ambient pressure structure. For this fit, we notice that whereas the average Ce-Ce bond does compress, the Ce-Al and the Ce-Cu shells expand or remain unchanged (within the error bars) which is irreconcilable with a "compressed" form of the ambient pressure phase. We also notice that the contribution to the total signal arising from the single Ce-Ce peak in this fit is largely "washed out" by a very large MSRD $\Delta\sigma^2_{Ce-Ce}$.

While, due to the limited k-range for the data, we are not able to distinguish a strong reduction of Ce-Ce partial coordination number from a strong increase in the Ce-Ce MSRD, the values reported in Table I for $\delta = 0$ are an indication that the local structure around Ce undergoes an important modification as a function of pressure that cannot be described by simple compression of the ambient pressure structure.

On the contrary, for the high pressure data, the quality of the fit improves very sharply for δ values approaching 0.3, and then gets worse again for larger values. This behaviour suggests that, always within this simplified model, a ≈ 0.3 Å split Ce-Ce shell describes the high pressure data better than a single Ce-Ce shell environment.

Figure 4 compares the data with the best fit curves (fit AP_1 for the ambient P data, and fit HP_2 for the high pressure data). Figure 5 (left and right) illustrate, for the ambient P data and for the high pressure data, respectively, the separate

TABLE I. Best fit structural parameters (errors bars in brackets) obtained for the EXAFS data at AP and HP for $Ce_{60}Al_{20}Cu_{20}$. δ is expressed in Å.

	Ambient P		High P	
Fit	AP_1 ($\delta = 0$)	AP_2 ($\delta = 0.28$)	HP_1 ($\delta = 0$)	HP_2 ($\delta = 0.28$)
χ^2_v	4.3	8.9	11.4	9.5
R_{Ce-Ce1} (Å)	3.54 (0.02)	3.58 (0.05)	3.43 (0.02)	3.48 (0.04)
R_{Ce-Ce2} (Å)	3.54	3.30	3.43	3.20
R_{Ce-Al} (Å)	3.19 (0.03)	3.08 (0.03)	3.28 (0.05)	3.43 (0.03)
R_{Ce-Cu} (Å)	3.23 (0.02)	3.33 (0.03)	3.19 (0.02)	3.18 (0.02)
$\Delta\sigma^2_{Ce-Ce}$ ($\times 10^{-3}$ Å^2)	29 (6)	18 (7)	40 (10)	24 (6)
$\Delta\sigma^2_{Ce-Al}$ ($\times 10^{-3}$ Å^2)	12 (4)	13 (3)	11 (4)	15 (1)
$\Delta\sigma^2_{Ce-Cu}$ ($\times 10^{-3}$ Å^2)	12	13	11	15

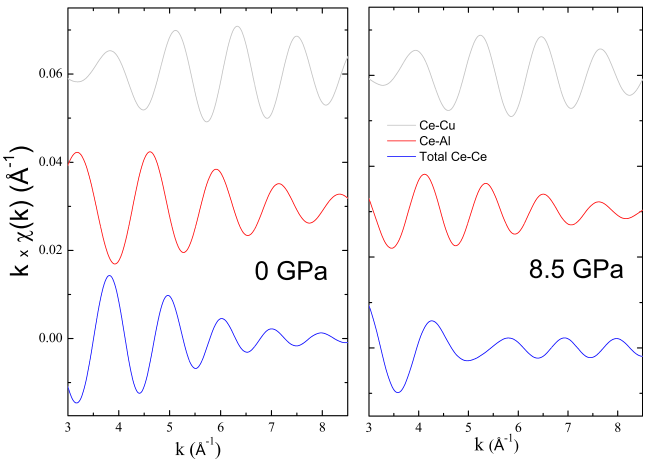

FIG. 5. Separate total Ce-Ce (blue), Ce-Al (red), and Ce-Cu(grey) EXAFS contributions to the total best fit k × χ(k) at 0 GPa (left) and 8.5 GPa (right).

contributions to the total fit: the total Ce-Ce (blue), the Ce-Al (red), and the Ce-Cu (grey).

Due to the low signal to noise ratio of the data, one could argue that the changes observed in the values of reduced χ^2_v between the "single-shell" and the "split-shell" environment are not significant, and that higher quality data are indeed required to definitively confirm these trends. Or, that fixing δ artificially "reduces" the error bars on the best fit parameters. This work, therefore, stimulates further experimental investigation of the high pressure behaviour of Ce-based BMGs. A larger k-range and a higher signal to noise ratio could not only permit to conclude with higher confidence on the splitting or not of the Ce-Ce distribution, but also test other structural models, look into more detailed structural details such as evolution under pressure of the partial coordination numbers.

In conclusion, we provide direct experimental evidence that local structural changes occur in compressed Ce-rich BMGs that cannot be described by simple compression. We observe a structural rearrangement compatible with a splitting of the Ce-Ce shell, in agreement with numerical simulations.[8] These local structural changes are accompanied by modifications in the electronic structure, whereby the Ce 4f states acquire a more delocalized character. This "electronically driven" polyamorphism involves, according to the Ce-Ce split-shell model, an important Ce-Ce bond shortening at the transition (almost 10% from this data analysis).

This is interestingly similar to pure cerium's behavior in which the 4f electron delocalization leads to an important volume collapse. In the latter transition, a study under high pressure and high temperature has revealed the existence of a CP at high temperature.[20] In order to probe the occurrence of a such CP in the phase diagram of a Ce-BMG, XANES measurements have also been performed in a $Ce_{69}Al_{10}Cu_{20}Co_1$ metallic glass under high pressure and high temperature (see Fig. 6). XANES recorded at 355 K (left panel—Figure 6) shows that the electronic delocalization upon pressure increase is almost completely reversible upon pressure release. The right panel of Fig. 6 shows XANES collected at 4 GPa during the compression and decompression cycle, at the two temperatures 300 K and 355 K. At 355 K, spectra recorded in the same thermodynamic conditions (P, T) at

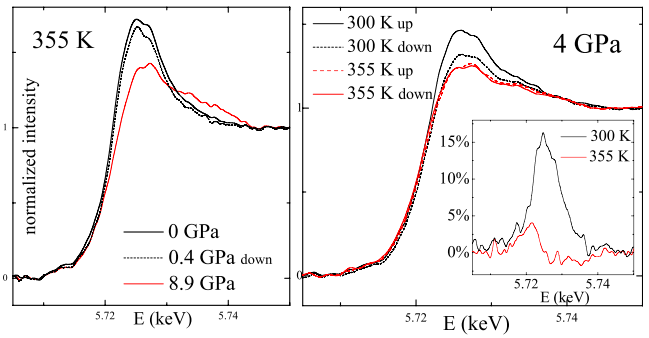

FIG. 6. Left: Ce L_3-edge XANES of $Ce_{69}Al_{10}Cu_{20}Co_1$ metallic glass at 355 K. Black: ambient, red: high P, dashed: after decompression. Right: XANES spectra on $Ce_{69}Al_{10}Cu_{20}Co_1$ at 300 K (black) and at 355 K (red). Continuous line: 4 GPa upon compression, dashed line: 4 GPa upon decompression. Inset: difference between the XANES at 4 GPa under compression and decompression divided by the compression spectrum (in%).

increasing and decreasing pressure are almost identical, while at 300 K a large hysteresis is observed. The inset, illustrating the relative difference between these XANES, highlights the shrinking of the hysteresis loop with temperature, from about 15% at 300 K to a few percent at 355 K. The strong reduction of the hysteresis loop is observed for temperatures higher than 320 K. The present shrinking of hysteresis loop at high temperature, also observed in pure cerium, is thus compatible with the existence at high temperature of a CP. This CP plays an important role in the two-scale theory of polyamorphism despite it has never been observed.[32] Hence, study of polyamorphism at extreme conditions in these materials opens an exciting area of research that could unravel the origin and mechanisms of polyamorphism.

We acknowledge G. Le Marchand and P. Munsch (IMPMC) for the DAC preparation and O. Mathon (Beamline Operation Manager), I. Kantor (beamline scientist), and technicians (S. Pasternak and F. Perrin) of the ESRF. We also thank Bruce Ravel for fruitfull discussions.

[1]W. H. Wang, Adv. Mater. **21**, 4524 (2009).
[2]J. C. Huang, J. P. Chu, and J. S. C. Jang, Intermetallics **17**, 973 (2009).
[3]E. Lutanie, Mater. today **12**, 12 (2009).
[4]B. Zhang, D. Q. Zhao, M. X. Pan, W. H. Wang, and A. L. Greer, Phys. Rev. Lett. **94**, 205502 (2005).
[5]J. F. Li, J. Q. Wang, X. F. Liu, K. Zhao, B. Zhang, H. Y. Bai, M. X. Pan, and W. H. Wang, Sci. China, Ser. G **53**, 409 (2010).
[6]B. Zhang, D. Q. Zhao, M. X. Pan, R. J. Wang, and W. H. Wang, J. Non-Cryst. Solids **352**, 5687 (2006).
[7]G. Marsh, Materials Today **6**, 38 (2003).
[8]H. W. Sheng, H. Z. Liu, Y. Q. Cheng, J. Wen, P. L. Lee, W. K. Luo, S. D. Shastri, and E. Ma, Nature Mater. **6**, 192 (2007).
[9]Q. Zeng, H. Sheng, Y. Ding, L. Wang, W. Yang, J. Z. Jiang, W. L. Mao, and H. K. Mao, Science **332**, 1404 (2011).
[10]Q. S. Zeng, Y. Ding, W. L. Mao, W. Luo, A. Blomqvist, R. Ahuja, W. Yang, J. Shu, S. V. Sinogeikin, Y. Meng *et al.*, Proc. Natl. Acad. Sci. U.S.A. **106**, 2515 (2009).
[11]Q. S. Zeng, C. R. Rotundu, W. L. Mao, J. H. Dai, Y. M. Xiao, P. Chow, X. J. Chen, C. L. Qin, H. K. Mao, and J. Z. Jiang, J. Appl. Phys. **109**, 113716 (2011).
[12]Q. S. Zeng, Y. Ding, W. L. Mao, W. G. Yang, S. V. Sinogeikin, J. F. Shu, H. K. Mao, and J. Z. Jiang, Phys. Rev. Lett. **104**, 105702 (2010).
[13]B. Zhang, M. X. Pan, D. Q. Zhao, and W. H. Wang, Appl. Phys. Lett. **85**, 61 (2004).
[14]M. Duarte, P. Bruna, E. Pineda, D. Crespo, G. Garbarino, R. Verbeni, K. Zhao, W. Wang, A. Romero, and J. Serrano, Phys. Rev. B **84**, 224116 (2011).
[15]Q. S. Zeng, Y. C. Li, C. M. Feng, P. Liermann, M. Somayazulu, G. Y. Shen, H. K. Mao, R. Yang, J. Liu, T. D. Hu *et al.*, Proc. Natl. Acad. Sci. U.S.A. **104**, 13565 (2007).
[16]Q. S Zeng, Y. Z. Fang, H. B. Lou, Y. Gong, X. D. Wang, K. Yang, A. G. Li, S. Yan, C. Lathe, F. M. Wu *et al.*, J. Phys.: Condens. Matter **22**, 375404 (2010).
[17]J. P. Rueff, J.-P. Itié, M. Taguchi, C. Hague, J.-M. Mariot, R. Delaunay, J.-P. Kappler, and N. Jaouen, Phys. Rev. Lett. **96**, 237403 (2006).
[18]H. L. Skriver, Phys. Rev. B **31**, 1909 (1985).
[19]G. Li, Y. Y. Wang, P. K. Liaw, Y. C. Li, and R. P. Liu, Phys. Rev. Lett. **109**, 125501 (2012).
[20]F. Decremps, L. Belhadi, D. Farber, K. Moore, F. Occelli, M. Gauthier, A. Polian, D. Antonangeli, C. Aracne-Ruddle, and B. Amadon, Phys. Rev. Lett. **106**, 065701 (2011).
[21]H. B. Lou, Y. K. Fang, Q. S. Zeng, Y. H. Lu, X. D. Wang, Q. P. Cao, K. Yang, X. H. Yu, L. Zheng, Y. D. Zhao *et al.*, Sci. Rep. **2**, 376 (2012).
[22]S. Klotz, T. Straussle, R. Nelmes, J. Loveday, G. Hamel, G. Rousse, B. Canny, J. Chervin, and A. Saitta, Phys. Rev. Lett. **94**, 025506 (2005).
[23]D. J. Lacks, Phys. Rev. Lett. **84**, 4629 (2000).
[24]H. W. Sheng, W. K. Luo, F. M. Alamgir, J. M. Bai, and E. Ma, Nature **439**, 419 (2006).
[25]B. Amadon, F. Jollet, and M. Torrent, Phys. Rev. B **77**, 155104 (2008).
[26]L. Belhadi, F. Decremps, G. Garbarino, G. Morard, and M. Mezouar (unpublished).
[27]H. K. Mao, J. Xu, and P. M. Bell, J. Geophys. Res. **91**, 4673, doi:10.1029/JB091iB05p04673 (1986).
[28]M. Newville, B. Ravel, D. Haskel, J. J. Rehr, E. A. Stern, and Y. Yacoby, Physica B **208**, 154–156 (1995).
[29]B. Zhang, R. Wang, and W. Wang, Phys. Rev. B **72**, 104205 (2005).
[30]M. O. Krause and J. H. Oliver, J. Phys. Chem. Ref. Data **8**, 329 (1979).
[31]E. A. Stern, Phys. Rev. B **48**, 9825 (1993).
[32]P. F. McMillan, J. Mater. Chem. **14**, 1506 (2004).